Egypt. J. Geol. 30, No. 1-2, pp. 89-108 (1986)

On the Formation of Skarn Rocks at Hammam Faraun, West Sinai, Egypt

Z. Abdel Kader and M.M. El Aref

Geology Dept., Faculty of Science, Cairo University, Giza, Egypt

THIS work constitutes an investigatory study of skarn rocks from Hammam area, and is a part of the larger project of examining the contact of basaltic rocks upon the enclosing sediments in the West Central Sinai. This research comprises the mineralogical and textural study of samples from the Tertiary basalt-dolerite sill and the surrounding Cretaceous limestones in order to determine the effect of the basaltic intrusion upon the country rock.

The nature and distribution of opaques within the intrusion and the metamorphosed rocks are studied using the reflecting microscope while rock analysis of samples from different parts of the sill and their calculated normative composition allowed the determination of the trend of differentiation of the basaltic rocks.

The skarn rocks are developed in layers of different mineralogical associations at the upper and lower contacts between the volcanics and the enclosing calcareous sediments. They have been classified into exoskarn and endoskarn according to their field position relative to the contact of the sill with the enclosing sediments. Exoskarns occur as banded rocks disposed along the upper and lower contacts and indicated as upper and lower exoskarns respectively. The most important skarn minerals identified are wollastonite, diospide, garnet, hedenbergite, vesuvianite, opaques, sphene and calcite. Endoskarns occur either as megascopic nodules distributed within the lower part of the sill or as microscopic xenoliths of amygdaloidal appearance confined to the upper zeolite-bearing zone.

The exoskarns were developed by contact metamorphism and metasomatism of Cretaceous limestone enclosing the dolerite sill. The endoskarns are probably produced by metasomatic infiltration through digested carbonate nodules.

This work constitutes an investigatory study of skarn rocks from Hammam Faraun area, and is a part of the larger project of examining the contact of basaltic rocks upon the enclosing sediments in the West Central Sinai. Gebel Hammam Faraun belongs to a highly faulted block which runs along the eastern shore of the Gulf of Suez (Fig. 1). The mountain cliffs rise over 500 m above the sea. The exposed rocks are mainly Cretaceous lime-

stones intruded by dolerite - basaltic sills and dykes of late Tertiary age.

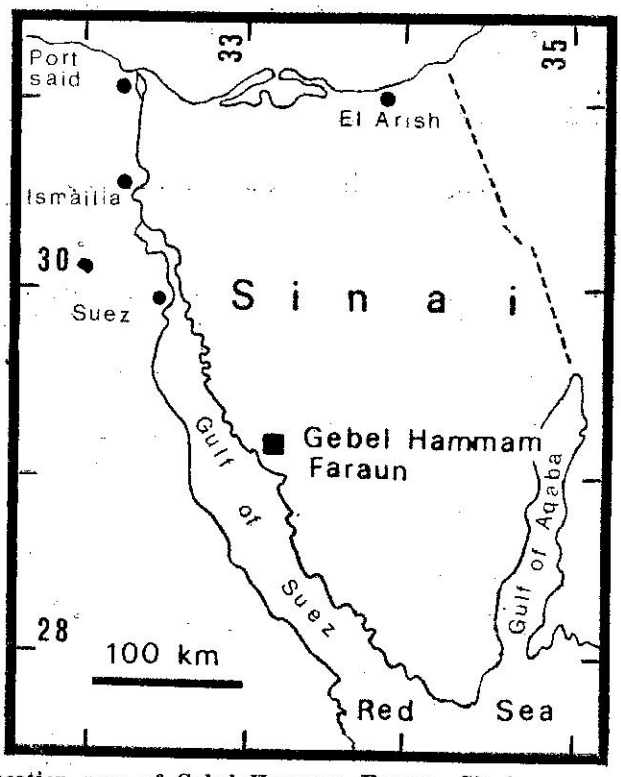

Fig. 1. Location map of Gebel Hamman Faraun, Sinai.

The samples used in this study were collected from the main sill south of the hot brines of Gebel Hammam Faraun as indicated on the stratigraphic sketch diagram (Fig. 2 and Fig. 3). This work comprises the mineralogical and textural study of samples from the sill and the surrounding country rocks. The nature and distribution of opaques within the intrusion and the metamorphosed rocks are studied using the reflecting microscope. Microprobe analysis of clinopyroxenes and wollastonite from the upper endoskarn have been carried out to determine the chemical characters of these minerals. Whole rock analysis of samples from different parts of the sill and their calculated normative composition allowed the determination of the trend of differentiation of these basaltic rocks. The mechanism of formation of the skarn rocks has been discussed.

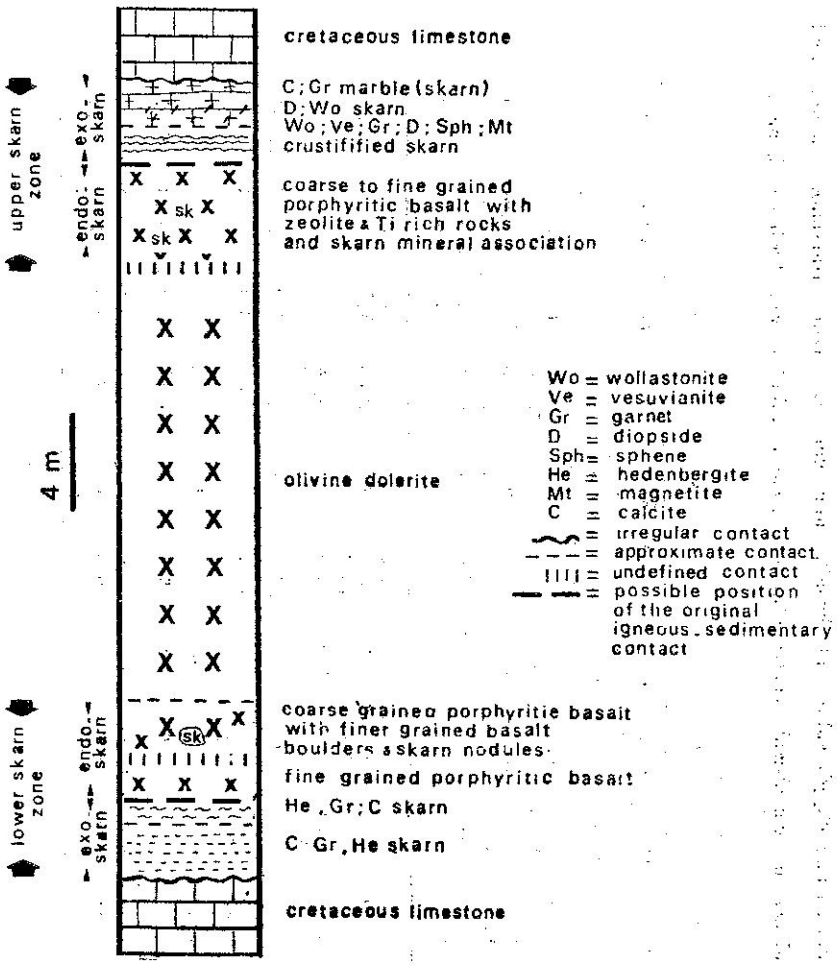

Fig. 2. Diagramatic section atross the dolerite sill showing the chilled porphyritic basalt borders and the lower and the upper skarn zones.

Olivine-dolerite sill

The olivine-dolerite is mainly of a non-porphyritic coarse-grained type with ophytic and intersertal textures (Fig. 4) in its central part, which grades upwards and downwards into chilled porphyritic basaltic rocks. The normative composition of the central doleritic mass (Table 1) is : 25% olivine; 15% nepheline; 20% diopside; 37% plagioclase (An_{60}) and 3.65% ilmenite. Under

TABLE 1. Chemical analyses, CIPW norms and Niggli values of basalts and dolerites from Hammam Faraun and Wadi Metallah Published analyses of world-wide continental and oceanic, alkaline and tholeiitic basalts.

	1	2	3	4	5	6	7	8	9	10	11	12	13	14
SiO_2	48.07	48.75	48.43	49.31	45.3	48.65	47.79	46.19	50.93	45.2	43.15	49.99	49.46	43.7
TiO_2	2.42	2.31	2.68	2.58	1.92	2.08	2.60	2.54	2.03	2.3	2.70	1.40	2.31	2.0
Al_2O_3	15.18	15.32	15.49	15.45	15.86	15.68	15,15	15.0	14.07	16.0	13.46	15.65	12.81	14.1
Fe_2O_3	2.84	5.18	8.22	4.96	0	10.38	3.77	2.70	2.88	6.5	4.52	1.74	4.14	6.7
FeO	8.69	7.15	4.09	7.40	9.94	1.88	8.68	9.01	9.06	8.1	8.22	8.06	8.77	7.3
MgO	7.87	6.79	6.06	7.18	11.81	9.33	7.62	9.05	6.34	7.6	10.80	7.98	6.32	5.95
CaO	10.59	9.71	9.90	8.96	9.65	9.72	10.10	10.82	10.42	9.3	9.80	11.36	10.97	10.80
Na_2O	3.01	3.57	3.65	2.60	4.54	1.05	2.87	2.78	2.23	3.2	3.47	2.70	3.01	2.50
K_2O	0.65	0.56	0.78	0.73	0.54	0.60	0.70	0.89	0.82	1.81	0.63	0.19	0.71	1.30
P_2O_5	0.49	0.49	0.51	0.57	0.27	0.44	0.50	0.38	0.23	0.39	0.75	0.13	0.35	0.40
Q	-	-	0.212	3.05	-	8.703	-	-	3.5	-	-	-	0.19	0.6
Or	3.86	3.32	4.62	4.62	3.19	3.548	4.15	5.6	5	5	9.63	1.1	4.2	7.69
Ab	25.45	30.20	30.87	21.98	10.71	8.87	24.31	19.4	18.9	26.2	9.67	23.1	25.47	21.15
An	25.99	24.10	23.57	28.2	21.3	36.31	26.38	25.6	25.9	26.7	16.34	29.8	19.35	23.42
Ne	-	-	-	-	15.0	-	-	2.3	-	0.3	10.67	-	-	-
Wo	9.75	8.7	9.3	5.24	10.36	3.78	8.55	Di20.7	20.2	13.4	22.23	21.0	26.67	22.08
En	8.83	12.5	15.08	17.88	6.41	23.24	11.95	-)	17.1	-	-	13.4	11.95	9.18
Fs	4.48	4.0	-	5.64	3.35	-	5.63	-)						
Fo	7.55	3.09	-	-	16.1	-	4.91)	16.6	-	13.3	16.76	5.5		
Fa	4.22	1.08	-	-	9.3	-	2.55)							
Mt	4.125	7.5	6.02	7.2	-	0.68	5.47	3.9	4.2	9.5	6.55	2.6	6.00	9.71
Hm	-	-	4.07	-	-	-	-	-	-	-	-	-	-	-
Il	4.59	4.38	5.09	4.9	4.38	9.91	4.94	4.9	3.8	4.4	5.13	2.7	4.39	3.79
Ap	1.16	1.17	1.20	1.34	1.17	3.94	1.18	0.9	0.5	1.0	1.64	0.3	0.83	0.94

cont/..

Table 1. cont.

	1	2	3	4	5	6	7
Al	19.92	20.8	21.44	21.41	18.51	20.76	20.02
Fm	47.4	46.42	44.16	48.9	51.6	52.70	48.5
C	25.27	23.97	24.92	22.6	20.49	23.4	24.25
Alk	7.42	8.8	9.48	7.09	9.40	3.14	7.25
Si	107.0	112.35	113.8	115.9	89.78	109.3	107.10
Ti	4.05	4.00	4.74	4.56	2.86	3.51	4.4
P	0.46	0.48	0.51	0.56	0.23	0.42	0.47
H	0	0	0	0	0	0	0
K	0.13	0.09	0.12	0.17	0.07	0.27	0.14
Mg	0.55	0.50	0.48	0.51	0.68	0.59	0.52

1.2: Coarse-grained porphyritic basalts from lower part of the sill.
3 : Coarse-grained porphyritic basalts from upper part of the sill.
4 : Very fine-grained porphyritic basalts from chilled margin.
5 : Coarse-grained dolerite , central part of the sill.
6 : Basalt dyke from Hammam Faraun area.
7 : Dolerite dykes from Wadi Matallah.
8 : Alkaline basalt (Nockolds et al., 1978).
9 : Tholeiitic basalt (Nockolds et al., 1978).
10 : Continental alkaline basalt (Varme, 1968).
11 : Alkaline basalt, Atlantic Ocean (Melson et al., 1967).
12 : Ocean-floor thoeleiitic basalt (Nockolds et al., 1978).
13 & 14: Basalts of attenuation zones (Gass, 1970).

TABLE 2. Microprobe analysis clinopyroxenes form the zeolite-bearing ba salts.

	1			2			3			4			5	
	Central	Int. Spot	Edge	Central	Int. Spot	Edge	Central	Int. Spot	Edge	Central	Int. Spot	Edge	Central	Edge
SiO_2	50.53	50.39	50.67	50.19	48.88	48.50	51.31	50.92	50.42	50.90	50.20	50.91	50.70	51.35
TiO_2	0.87	1.09	1.02	1.25	1.79	2.05	0.53	0.68	0.92	0.93	0.92	0.96	0.64	0.70
Al_2O_3	1.46	1.71	1.60	2.18	4.74	4.27	0.83	1.11	1.25	1.47	1.40	1.70	1.05	1.09
FeO	13.61	14.72	14.17	13.07	9.99	8.83	15.88	14.97	14.61	14.01	13.64	12.93	15.69	16.11
MnO	0.37	0.33	0.33	0.31	0.09	0.05	0.53	0.64	0.41	0.38	0.37	0.45	0.41	0.44
MgO	12.23	12.25	12.36	12.80	11.88	12.94	11.59	12.70	12.24	13.03	12.88	13.24	12.77	12.62
CaO	19.03	19.16	18.27	19.92	21.56	21.79	18.87	18.47	18.77	19.19	19.18	19.43	17.70	17.35
Na_2O	0.32	0.35	0.36	0.35	0.28	0.33	0.40	0.25	0.27	0.30	0.34	0.33	0.30	0.31
K_2O	0.03	0.00	0.01	0.00	0.01	0.00	0.00	0.00	0.06	0.01	0.01	0.00	0.04	0.00
Cr_2O_3	0.04	0.08	0.00	0.01	0.02	0.09	0.05	0.00	0.05	0.06	0.00	0.00	0.00	0.00
Total	98.50	100.8	99.79	99.77	99.23	98.85	99.98	99.79	99.71	100.28	98.94	99.95	99.30	99.98
Wo	40.53	39.96	38.40	40.97	46.92	46.64	39.5	38.2	39.5	39.5	39.9	40.2	36.9	36.3
En	36.24	35.54	36.16	37.21	35.96	38.53	33.7	36.5	35.8	37.3	37.3	38.	37.	36.7
Fs	23.24	24.51	25.44	21.82	17.12	14.83	26.8	25.2	24.7	23.0	22.8	21.6	26.1	27.0
FeO^T/MgO	1.11	1:20	1.22	1.02	0.84	0.68	1.37	1.18	1.19	1.07	1.06	0.97	1.22	1.27
FeO^t/MgO liq.	4.76	5.06	5.15	4.30	3.54	2.87	5.78	4.98	5.02	4.51	4.47	4.09	5.18	5.38

Fig. 3. Field photograph showing the dolerite sill and the lower exoskarn zone.

Fig. 4. Olivine surrounded by plagioclase forming intersertal texture. Large plate of augite in the left part of the photo coarse-grained dolerite. X-Nicols.

the microscope, olivine is usually altered to serpentine, chlorophaeite, iddingsite, celadonite and minor talc. In this level of the sill, ilmenite with subordinate titanomagnetite, forms discrete idiomorphic crystals occupying interstitial spaces between the silicates or enclosed within olivine and pyroxene crystals. They form also myrmekitic texture with the silicates. The occurrence of titanomagnetite crystals distinctly increases towards the lower part of the sill. It forms together with homogeneous ilmenite and their oxidation products the main opaque mineral association. Ilmenite intergrowth in titanomagnetite forms mainly trellis types (Budington and Lindsley, 1964). Composite and sandwich inter-

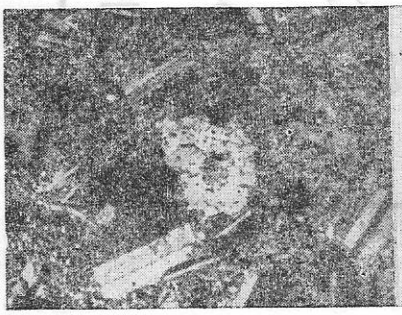

Fig. 5. Porphyritic basalt. Phenocrysts of plagioclase and augite in a finegroundmass. X-Nicols.

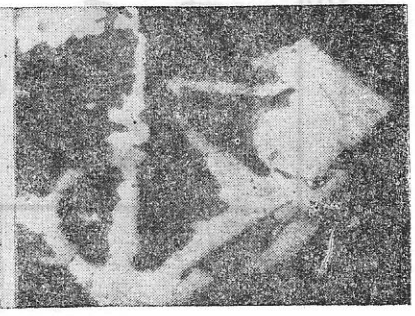

Fig. 6. Skeletal crystals of opaques in chilled basalts. Polished section.

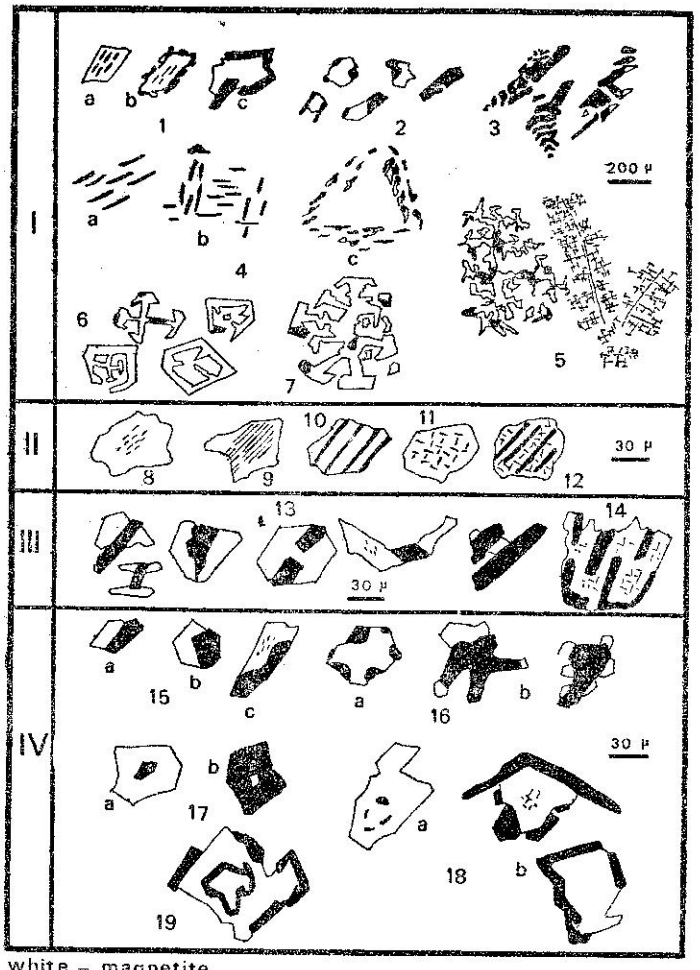

Fig. 7.

Fig. 7. Schematic representation showing the main external fabrics of ilmenite (black) and magnetite (white) in the porphyritic basalts (group I) and their internal geometric intergrowth patterns (groups II, III and IV).
Group I : Small rod-like ilmenite crystals with or without magnetite arranged either parallel to the plagioclase twin lamellae (1 a) ; interruptedly distributed around the plagioclase crystals (1 b) or included in or coating the pyroxenes (1 c). Type 2 = isolated grains or idiomorphic crystals consisting of ilmenite and magnetite or homogeneous ilmenite. Type 3 = discrete ilmenite crystals with or without magnetite. Type 4 = shredded or skeletal growth crystals of ilmenite with or without magnetite arranged in parallel to subparallel pattern (4 a), rectilinear pattern (4 b) or triangular pattern (4 c) which may follow pyroxene boundaries. Type 5 = branched or dendritic titanomagnetite crystal growth which are evenly or haphazardly initiated at terminations and along primary, secondary or tertiary cross arms. Type 6 = titanomagnetite of cruciform morphologic pattern. Type 7 = skeletal titanomagnetite crystals of multiple cross-arm type. Types 5, 6 and 7 are the main common types of group I.

Group II : displays grains of trellis intersprowths of ilmenite in titanomamgnetite. Ilmenite lamellae occur as spindle shape (type 8); parallel thin lamellae (type 9); partially thick exsolved lamellae (type 10) and network (widmanstatten) texture (type 11) or represent super trellis pattern infilled by several generations of finer ilmenite lamellae (type 12).

Group III : displays sandwich (type 13) and banded lamellar (type 14) intergrowths of ilmenite and titanomagnetite.

Group IV : includes grains of composite (granular) intergrowth types. Type 15 = composite pattern of ilmenite and magnetite in juxtaposition and showing rectilinear, polygonal or curved contacts (types 15 a, b and c respectively). Type 16 = mottled intergrowth patterns. Type 17 = granular intergrowth of internal (17 a) or external (17 b) patterns. Type 18 = atoll structure of ilmenite in magnetite (type 18 a) or concentric ilmenite crystals surrounding magnetite (type 18 b). Type 19 = concentric or multiple shell intergrowth of ilmenite and magnetite.

growths are less abundant. The trellis intergrowths are considered to be an earlier oxidation product of original magnetite - ulvospinel solid solution (Basta, 1959; Vincent, 1960); Budington and Lindsley, 1964 and Haggerty, 1967a), whereas the sandwich and composite intergrowth are products of either oxidation or primary crystallization from the melt (Haggerty, 1976a). Both the titanomagnetite and ilmenite grains are commonly oxidized producing pseudomorphic oxidation associations. The oxidation processes are displayed by the formation of exsolved minute spinel rods in titanomagnetite and ferrirutile into ilmenite (metailmenite) and the development of mottling appearance of ilmenite. A progressive decomposition stage leads to the formation of rutile-titanohematite-ferriilmenite assemblage with or without relics of ilmenite.

The chilled margins consist of porphyritic basalts, plagiophyric with subordinate amount of clinopyroxenes and olivine. The groundmass varies from coarse-grained to glassy (Fig. 5). The normative composition of these rocks consists of plagioclase amounting from 42 to 56% (An_{40}-An_{60}); clinopyroxene from 10 to 17%; olivine 0 to 11% : ilmenite 4.6 to 5% and magnetite 4 to 7%. Normative hematite is recorded in the upper chilled margin only (Table 1). In these rocks, ilmenite and titanomagnetite are prominently developed in skeletal crystals (Fig. 6) most probably related to the rapid rate of cooling and the onset of co-crystallization of silicates (Haggerty, 1976b). The main external morphologic patterns and the internal intergrowth types of the ilmenite and titanomagnetite are illustrated and described in Fig. 7. The sandwich and composite intergrowth patterns are more abundant than the trellis type. Oxidation products are rarely observed. The sandwich and composite intergrowths in these rocks seem to be developed during primary crystallization rather than oxidation of a primary ulvospinel-magnetite solid solutions (Buddington and Lindsley, 1964) or subsolidus diffusions (Vincent *et al.*, 1954 and Wright, 1964). This conclusion is based on the following observational evidences : a) the existence of the three textural types ; b) the extension of ilmenite arms from the sandwich and composite types into the groundmass; c) the absence of spinel product and the rare evidence of oxidation of the three types; d) the sharp termination of ilmenite at the sandwich and composite titanomag-

Fig. 8. Polysynthetic triangular twinning of analcite filling cavities. Amygdaloidal basalt. X-Nicols.

Fig. 9. Brown sphene (Sp) and six-sided apatite phenocrystals surrounded by plagioclase. Ordinary light.

netite-ilmenite interface and, e) the myrmekitic intergrowth between the opaques and the surrounding silicates.

In the upper chilled zone, about 4 m below the upper contact, a band of highly amygdaloidal porphyritic basalt shows strong titanium enrichment. These rocks are pyroxene-phyric; plagioclase in much subordinate and highly altered. The large amygdules are filled with fibrous zeolite, calcite, analcite and tile-structure cristobalite (Fig. 8). The Ti-enrichment is displayed by the formation of large phenocrysts of sphene (Fig. 9) and the colour and chemical zoning of purplish titaniferous augite. These rocks

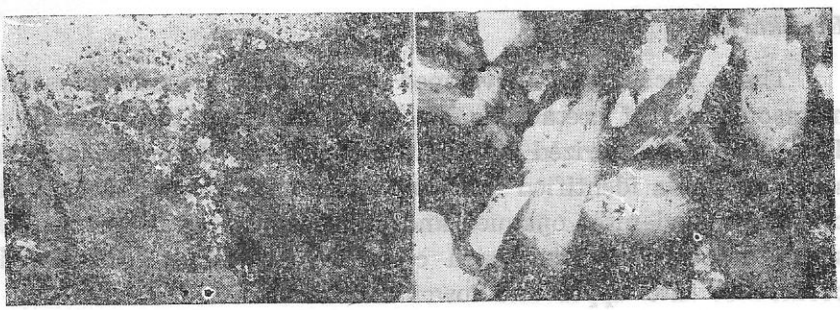

Fig. 10. Crustified upper exoskarn in thin section. Ordinary light.

Fig. 11. Coarse idioblasts of zoned diopside, colourless wollastonite and black magnetite.

are also characterized by the occurrence of xenoliths of calc-silicate mineral assemblages surrounding brown zoned clinopyroxenes, The microprobe analysis of these pyroxenes (Table 2) plot in the augite-salite fields on the ternary diagram of Poldervaart and Hess (1951). The calculated FeO/MgO ratio of the liquid using the partition coefficient value of 0.24 for clinopyroxene-liquid (Church and Riccio, 1977) ranges from 2.87 to 5.78 (Table 2) suggesting that this liquid is quite fractionated. Consequently, these amygdaloidal rocks probably represent an advanced stage of crystal fractionation of the primary magma composing the bulk of the dolerite sill with FeO/MgO ratio ranging from 0.84 to 1.89.

The opaque minerals in these rocks are represented mainly by ilmenite and titaniferous magnetite. The opaques form discrete elongated crystals and commonly exhibit myrmekitic and concentric coating intergrowth types with the pyroxenes. Blebs of ilmenite are usually distributed within the plagioclase twin lamellae. These geometric intergrowth relationships emphasize the primary co-crystallization of ilmenite and titaniferous magnetite with the silicates.

Skarn rocks

Skarn rocks have been classified into exoskarn and endoskarn according to their field position relative to the contact of the sill with the enclosing sediments. Exoskarns occur as banded rocks of different mineralogical composition, disposed along the upper and lower contacts, while the endoskarn represents mineral assemblages enclosed within the volcanics and forming nodular bodies.

Exoskarns

These rocks were developed by contact metamorphism and metasomatism of cretaceous limestone enclosing the doleritic sill. They are characterized by light colouration. The most important skarn minerals identified are wollastonite, diopside, garnet, hedenbergite, vesuvianite; opaques and sphene are less frequent. These skarn associations have been classified according to their field occurrence into upper and lower exoskarns.

The upper exoskarns are represented mainly by a thin crustified skarn zone followed upwards by a calcite-garnet skarn layer. The crustified skarn type is composed of successive alternating

microscopic crusts of different minerals associations (Fig. 10) including : wollastonite-diopside; wollastonite-vesuvianite; garnet-wollastonite-sphene with minor hedenbergitic pyroxene and opaques. The mineral association of each crust shows distinct idiomorphic termination; zonation and increase in the grain size towards the next successive crust.

Wollastonite occurs as large unzoned idioblasts set in a fine mosaic texture. The electron microprobe analysis of these large crystals (Table 3) shows that their FeO content falls within the range of iron wollastonite (Deer *et al.,* 1978). It occurs also as fibrous and wavy aggregates interstitial to garnet crystals. The fine wollastonite crystals may be poikilitically enclosed in diopside.

Diopside pale brown, zoned, extinction angle 38°C, forms granoblastic mosaic with the twinned wollastonite (Fig. 11).

Vesuvianite forms small rounded brown grains unzoned and characterized by anomalous blue interference colours. It is sometimes enclosed within the wollastonite prophyroblasts.

Garnet occurs as brown anhedral crystals slightly anisotropic disseminated with isotropic cublets. It forms also earthy bands enclosing degraded brown sphene crystals (Fig. 12).

Hedenbergitic pyroxene forms small plates, pale green with prismatic cleavage and low birefringence, interstitial between wollastonite, vesuvianite and garnet.

Opaques are represented mainly by sulphides and magnetite. The sulphides consist of minute aggregates of pyrite, pyrrhotite, chalcopyrite and sphalerite. These aggregates are usually scattered along the convex surfaces of the skarn crusts. Pyrrhotite is commonly altered to marcasite. Magnetite is essentially distributed with wollastonite-diopside bands mantling the silicates.

Calcite-garnet skarn (or marble) layer is composed mainly of blocky calcite and grossularite (Fig. 13) and grades upwards into unmetamorphosed limestone (Fig. 13).

Lower exoskarns

The first layer underlying the sill consists of a partially consolidated and bedded green rock, composed of hedenbergitic pyro-

xene, garnet and minor interstitial calcite. Hedenbergitic pyroxene; containing up to 5% FeO, forms long prismatic fractured green crystals in radiating aggregates with 42% extinction angle (Fig. 14). The garnet forms isotropic anhedral yellowish brown crystals usually lined by minute crystals of magnetite. The underlying layer is composed essentially of blocky calcite with subordinate amounts of minute garnet crystals and fan-shaped hedenbergite aggregates (Fig. 15).

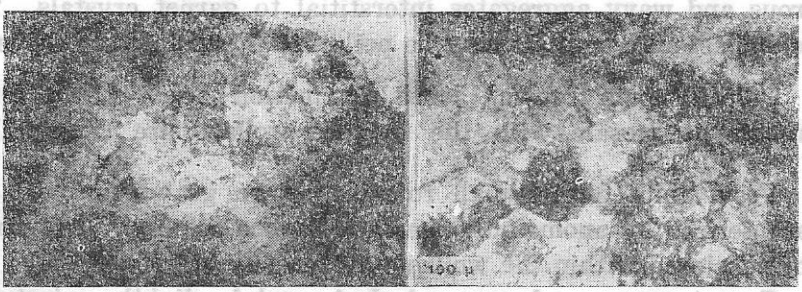

Fig. 12. Garnet (grey to dark-grey), metamorphic sphene, (black) and calcite (white). Ordinary light.

Fig. 13. Octahedral cracked grossularite in blocky calcite. Upper exoskarn. Ordinary light.

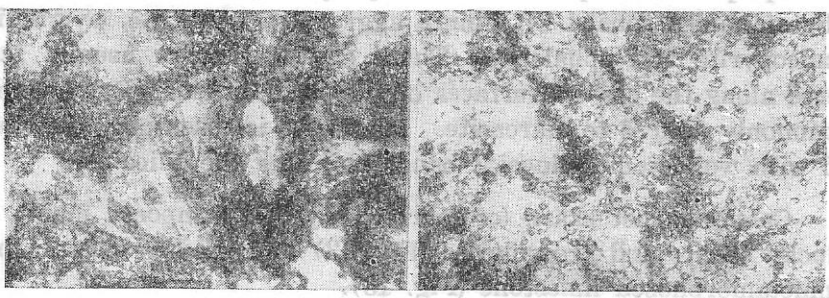

Fig. 14. Prismatic hedenbergite (dark grey) and interstitial calcite (white). Lower exoskarn. Ordinary light.

Fig. 15. Minute grossularite ; fibrous hedenbergite (dark grey) and calcite (white). Lower exoskarn. Ordinary light.

Endoskarns

Endoskarns occur either as megascopic nodules distributed within the lower porphyritic basalts or as microscopic xenoliths of amygdaloidal appearance confined to the upper zeolite bearing titanium rich volcanic rocks.

Lower endoskarns

The skarn nodules are of spherical and ellipsoidal shapes, up to 20 cm in diameter. They are always of white to light-grey colour and usually surrounded by fractured aureoles (Fig. 16). Microscopically these nodules consist of wollastonite, titaniferous vesuvianite, hedenbergitic pyroxene and garnet. Wollastonite occurs in two main morphological generations including fine granular aggregates and prismatic idioblasts. Vesuvianite forms large plates exhibiting strong pleochrism from yellow to purplish brown and anamolous blue interference colours. These large plates enclose poikilitically fine aggregates of wollastonite. Anhedral crystals of hedenbergitic pyroxene are usually associated with the prismatic wollastonite (Fig. 17). Garnet occurs as subhedral brown crystals disseminated with iron oxide inclusions. It forms also idiomorphic octahedral cracked crystals showing yellow core and colourless outer zones. Fine-grained granoblastic and poikiloblastic are the main textures characterizing these skarn nodules.

Upper endoskarn

The upper endoskarn, formed within the zeolite-bearing titanium rich zone, represents tiny xenoliths of limestone digested by the rising lava. It consists of coarse aggregates of wollastonite surrounded by dark brown, zoned idiomorphic pyroxenes. These pyroxenes are of titaniferous augite-salite composition ranging from $Ca_{36}\ Mg_{37}\ Fe_{27}$ to $Ca_{47}\ Mg_{39}\ Fe_{14}$. Euhedral crystals of magnetite are intimately associated with wollastonite (Fig. 19).

Discussion and Conclusion

To explain the metasomatic production of skarn rocks, numerous investigators (Bowen, 1940; Khorzinsky, 1948; Burnham, 1959; Kennedy, 1959; El Sharwaki, 1964; Reverdatto, 1970 and Winkler, 1979) assume that the elements diffuse in opposite directions from

Fig. 16. Field photo of lower endoskarn nodule surrounded by cracked aureole.

Fig. 17. Titaniferous vesuvianite (grey), wollastonite (white) from the lower endoskarn. Ordinary light.

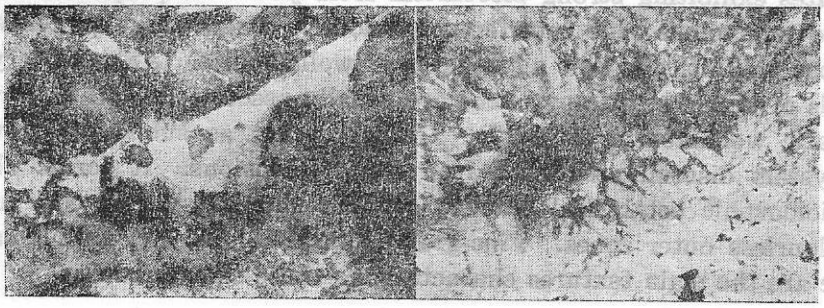

Fig. 18. Magnetite (black) zones diopside (grey) and coarse wollastonite (white). Diopside enclosed in wollastonite. Ordinary light.

Fig. 19. Upper endoskarn. Magnetite (black) surrounded by wollastonite (white) and idioblasts of metamorphic pyroxenes. Ordinary light.

the intrusive body towards the enclosing carbonates and vice versa, from the areas of high concentration to zones of low concentration. Exchange reactions between the different compounds along the diffusion front would produce the lime-silicate minerals of the skarns. As the diffusing elements differ in mobility, they reach the diffusion front at different rates producing the zonal arrangement of the skarn mineral assemblages.

At Hammam Faraun, the upper and lower exoskarns differ markedly in composition. It may be noticed that wollastonite, diop-

side and vesuvianite which are the essential components of the upper exoskarns, are completely absent from the lower exoskarns. The latters are composed mainly of hedenbergitic pyroxene and garnet with calcite. This variation in composition is due to the following factors :

1. The difference in composition of the overlying and underlying sediments.
2. The differing rate of diffusion of the various elements.
3. The variation in concentration of volatiles in the upper and lower parts of the sill.

The formation of hedenbergite-grossularite in the lower exoskarn indicates that the underlying sediments are probably ferrodolomites with argillaceous intercalations since :

$$Ca\ (Fe,Mg)\ (CO_3)_2 + 2\ SiO_2 \longrightarrow Ca\ (Fe, Mg)\ Si_2O_6 + 2\ CO_2$$

ferrodolomite hedenbergite

The formation of hedenbergitic pyroxene suggests the presence of a reducing medium allowing high concentration of ferrous iron along the exogenous boundary. The absence of wollastonite from the lower exoskarns can be explained by the fact that the PCO_2 was locally increased preventing the development of this mineral (Kennedy, 1958), since :

$$CaCO_3 + SiO_2 \longrightarrow Ca\ SiO_3 + CO_2$$

The increase of the PCO_2 was further confirmed by the presence of oxidation products of the opaque minerals in the lower part of the sill. In fact, the development of these oxidation products in this interior level of the sill can be related to migrating isotherms as function of the cooling rate (Wright, 1961; Watkins and Haggerty, 1967 and Sato, 1972). These products may indicate the difference in the oxygen fugacities (FO_2) which were sufficient to introduce the first oxidation «exsolution» lamellae of ilmenite in titanomagnetite or later, pseudomorphic oxidation and demonstrate the tendency of volatile accumulation, dissociation of H_2O and loss of hydrogen during prolonged cooling (Haggerty, 1971 and 1976). This loss of hydrogen at the lower part of the sill may justify the presence of the reducing medium at the lower exoskarn.

At the upper contact the pressure of the overlying rocks is much reduced allowing free circulation of CO_2 derived by decarbonation of the enclosing sediments and formation of wollastonite. The concentration of magnetite and minute sulphide crystals in the crustified exoskarn is consistent with the fact that the relative mobility of certain elements, including iron, changes with falling temperature (Zharikov, 1968). At low temperature, the mobility of iron is much reduced leading to the accumulation of magnetite. At a lower temperature stage, mobile sulphur and copper may react with iron becoming completely inert, producing the sulphide minerals. The absence of hedenbergitic pyroxene and the formation of diopside in the upper exoskarns is probably due to the fact that the overlying sediments are dolomitic limestones rather than ferrodolomite.

Endoskarns are probably produced by metasomatic infiltration through digested carbonate nodules (Kennedy, 1959). The most important elements migrating from the lava towards the nodules being silica and titanium.

The metastomatic effect of Egyptian Teritiary basalts upon enclosing sediments has been previously studied in Gebel Abu Treifiya by El Sharkawi and Abu Khadra, (1968). Wollastonite and diopside were the main calc-silicate minerals recorded.

It may be concluded that the mineralogical and textural relations in the skarn rocks from Gebel Hammam Faraun are consistent with their derivation by metasomatic infiltration processes. The results of this study are encouraging for further investigation for possible occurrence, distribution and economic importance of skarn deposits in Western Sinai.

Acknowledgements

The authors are greatly indebted to Dr. El Sharkawi and Dr. El Gabi for fruitful discussions. We thank deeply Dr. Abu Khadra and Dr. Darwish for their help in the sampling. Dr. El Bayoumi is acknowledged for analyzing the samples.

References

Basta, E.Z. (1959) Some mineralogical relationships in the system Fe_2O_3-Fe_3O_4 and the composition of titanomaghemite. Econ. Geol., Vol. 54, p. 698.

Bowen, N.L. (1940) Progressive metamorphism of siliceous limestone and dolomite, J. Geol., Vol. 48, p. 225-274.

Buddington, A.F. and Lindsley, D.H. (1964) Iron-titanium oxide minerals and synthetic equivalents. J. Petrol., Vol. 5, p. 310-357.

Burnham, C.W. (1959) Contact metamorphism of magnesian limestone at Grestmore California, Geol. Soc. Am. Bull., Vol. 70, p. 879-920.

Church, W.R. and Riccio, L. (1977) Fractionation trends in the Bay of New Founland. Polycyclic cumulate sequences in ophiolites and their classification. Can. J. Earth. Sci., Vol. 14, p. 1156-1165.

Deer, W.A., R.R. and Zussman, J. (1978) «Rock Forming Minerals», Vol. 2A : Single chain silicates. Longman Group Ltd., London, p. 668.

El Sharkawi, M.A. (1964) Pyrometasomatic ore deposits in Lower Culm Measure of North-West Dartmoor Devonshire, England, Ph. D. Thesis, University of Newcastle-Upon-Tyne, p. 162.

El Sharkawi, M.A. and Abou Khadra, A.M. (1968) The dolerite-limestone contact of Gebel Abou Treifiya, Cairo-Suez District. Egypt. J. Geol., Vol. 12, p. 11-19.

Haggerty, S.E. (1971) High-Temperature Oxidation of Ilmenite in Basalts. Ann. Rep. Dir. Geophys. Lab. Year Book 70, p. 165.

Haggerty, S.E. (1967 a) Oxidation of Opaque Mineral Oxides in Basalts, in Rumble, D. (ed.). Oxide Minerals, Min. Soc. Am., Vol. 3, Hg 1-100.

Haggerty, S.E. (1976 b) Opaque Mineral Oxides in Terrestrial Igneous Rocks, in Rumble, D. (ed.) : Oxide Minerals, Min. Soc. Am., Vol. 3, Hg 101-300.

Kennedy, W.Q. (1959) The formation of a diffusion reaction skarn by pure thermal metamorphism. Min. Mag., Vol. 32, p. 26-32.

Korzhinsky, D.S. (1948) The petrology of the Turin Skarn Copper Dpt. Trudy I.G.N. AN SSSR, 68.

Poldervaart, A. and Hess, H.H. (1951) Pyroxenes in the crystallization of basaltic magmas. J. Geol., Vol. 59, p. 472-489.

Reverdatto, V.V. (1970) Pyrometamorphism of limestones and the temperature of basaltic magmas, Lithos, Vol. 3, p. 135-43.

Sato, M. (1972) Intrinsic oxygen fugacities for iron-bearing oxide and silicate minerals under low total pressure. Geol. Soc. Am. Mem. 135-289.

Vincent, E.A. (1960) Ulvospinel in the Skaergaard intrusion, Greenland. Neues Jahrb. Mineral, Abh., 94, 993.

Watkins, N.D. and Haggerty, S.E. (1967) Primary oxidation variation and petrogenesis in a single lava. Contrib. Mineral. Petrol. 15, 251.

Winkler, H.G.F. (1979) «Petrogenesis of Metamorphic Rocks». Springer-Verlag, New York, Heidelberg Berlin, p. 348.

Wright, J.B. (1961) Solid-solution relationships in some titaniferous iron oxide ores of basic igneous rocks, Min. Mag., Vol. 32, p. 778.

Zharikov, V.A. (1968) Skarn deposits. In «Genesis of Endogenous Ore Deposits,» Smirnov, V. I. (Ed.). Moscow, Nedra, p. 22-302.

تكوين صخور الاسكارن بمنطقة حمام فرعون غرب سيناء ، مصر

زينب عبد القادر ومرتضى مراد العارف

قسم الجيولوجيا ، كلية العلوم ، جامعة القاهرة ، الجيزة ، مصر

تصاحب صخور الاسكارن بركانيات البازلت ـ دوليرت التابعة للعصر الثلاثى بمنطقة جبل حمام فرعون بسيناء ، تتميز البركانيات بالتطابق مع وجود صخور حاملة للزيوليت وغنية بالتيتانيوم بالمنطقة العليا والسفلى فى الجسم البركانى .

وقد تكونت صخور الاسكارن فى شكل طبقات ذات تركيبات معدنية مختلفة عند خطى الالتقاء العلوى والسفلى بين البركانيات والصخور الجيرية الحاوية لها . وتعتبر معادن الولاستونيت ، الفيزوفيانيت ، الجروسيولاريت الهدنيرجيت ، الديوبسيد ، السفين ، الكلسيت ، والمجنتيت أهم معادن السكارن التى تم التعرف عليها . وقد ناقش البحث كذلك طريقة تكوين هذه الصخور .